Hybrid Method of Remote Sensing of Electrostatic Potential for Proximity Operations

Kieran Wilson
Graduate Research Assistant
Aerospace Engineering Sciences
University of Colorado Boulder
Boulder, Colorado 80303
kieran.wilson@colorado.edu

Miles Bengtson
Graduate Research Assistant
Aerospace Engineering Sciences
University of Colorado Boulder
Boulder, Colorado 80303

Hanspeter Schaub
Glenn L. Murphy Endowed Chair
Aerospace Engineering Sciences
University of Colorado Boulder
Boulder, Colorado 80303

Abstract—Touchless determination of electrostatic potential is an enabling technology for a wide variety of orbital robotics applications. This concept is useful for characterizing satellite surfaces during servicing missions, preventing electrostatic discharge during initial contact, and accounting for electrostatic perturbations that affect the relative motion during proximity operations. The electrostatic tractor concept proposes using these forces and torques to detumble or tow uncontrolled satellites to graveyard orbits. All of these applications require the ability to remotely sense the voltage on another spacecraft prior to any physical contact. Two methods have been proposed for remote monitoring of spacecraft electrostatic potential from a co-orbiting craft. This paper considers fusing data from both sensing methods to mitigate the limitations of each method and produce a robust estimate of the surface voltage. The methods involve observing x-ray and electron spectra emitted when energetic electrons, such as those from an electron gun, strike the surface of the target. The electron method provides a highly accurate estimate but is strongly sensitive to the relative geometry of the spacecraft which limits the times during which a usable signal is received. The x-ray method produces a less accurate estimate but is less affected by the target geometry. Experimental results demonstrate that fusing the datasets produces significant improvements in accuracy and geometrical coverage of the voltage estimate across a wide range of conditions, including a rotating target plate. These results are important for future missions which must remotely monitor the potential on a nearby object to ensure mission success.

TABLE OF CONTENTS

1. INTRODUCTION AND MOTIVATION

As the space industry considers increasingly complex missions with multiple spacecraft operating in close proximity, there is need to be able to remotely characterize an orbital object from a nearby spacecraft. Ambient plasma fluxes and the photoelectric effect cause satellite surfaces to become electrically charged, up to thousands of volts in polar low Earth orbit (LEO) or 10s of kV in the hot, sparse plasma environment at geosynchronous orbit (GEO) (1; 2). Even though proximate satellites experience the same ambient space weather conditions, they may charge to different po-

tentials because charging depends strongly on the material properties. Further, unique geometries experience different sunlight exposure and thus photoelectron currents (3). As a result, there is a significant risk for potentially hazardous electrostatic discharge during initial contact. Additionally, the charged craft create electrostatic forces and torques which affect the relative motion. Therefore, it is imperative that future multi-spacecraft missions have a means for remotely characterizing the electrostatic state of another object. The application of remote electrostatic characterization to specific mission architectures is discussed below.

Robotic servicing and salvaging missions propose operations in which a satellite approaches and then interfaces with a retired satellite, such as SpaceLogistics' Mission Extension Vehicle (MEV), which is designed to take over station keeping and attitude control for an out of fuel GEO communications satellite, and NASA's Restore-L mission to refuel Landsat-7 (4; 5; 6). These missions require satellites to operate in very close proximity and eventually make contact. Many of these servicing concepts are focused on GEO because of the high value of operating GEO assets. Some planned missions require rendezvous and docking in orbital regimes which lead to large surface potentials on spacecraft. NASA's planned Lunar Gateway program involves spacecraft docking in the outer radiation belt to transfer modules to lunar orbit. Reference (7) shows that expected potential difference between the Lunar Gateway and Orion module prior to making contact is on the order of kilovolts. In Reference (8), a tradespace is defined of eight mission architectures for on-orbit servicers and assemblers. Any scenario involving two or more objects in close proximity without a direct conductive path between them would benefit from electrostatic sensing. Such is the case for six of the eight defined architectures for on-orbit assemblers and servicers.

Additionally, the valuable GEO region is becoming increasingly congested and the need for active debris remediation is well-established. Some orbital servicing or debris removal concepts propose leveraging the electrostatic forces and torques between multiple craft to control relative dynamics without making physical contact. The electrostatic tractor is an elegant solution for remediation of debris from valuable orbital slots in GEO (9). The tractor craft approaches the debris object and directs an electron beam toward it to transfer charge. Subsequently, the tractor charges positively and the debris object charges negatively, which produces a resultant attractive force. The tractor then uses inertial thrusters to tug the debris object to a graveyard orbit without ever requiring physical contact. Both tugging and pulling configurations have been investigated (10). Similarly, electrostatic torques can be used to detumble large objects prior to approach for servicing. This is critical because defunct GEO spacecraft and debris objects can have rotational rates of up to 10s of

degrees per second (11; 12; 13), which prohibits attempts to physically interface with them for servicing or re-orbiting. Electrostatic control of another object requires knowledge of the forces and torques, which in turn depend on the voltages and capacitances.The capacitance of a spacecraft body is typically taken to be a function of the geometry alone, so if potentials and the spacecraft geometries are known, then the intercraft forces and torques can be evaluated using a method like the Multi-Sphere Model (MSM) (14). Therefore, if the surface potential on the target craft can be evaluated, then the dynamics of the system can be computed. Remote electrostatic characterization is an enabling technology for a wide range of on-orbit servicing, salvaging, and rendezvous applications.

Two promising methods for remote electrostatic characterization are reviewed in this paper. The first method involves using the servicing craft to measure the energy distribution of secondary electrons and photoelectrons emitted by the object of interest. Both types of electrons are emitted with initial energies of a few eV, so the energy with which the electrons arrive at the servicing craft is equal to the potential difference through which they have been accelerated (plus their very small initial energy). Given the potential of the servicing craft, the potential of the target object is inferred (15; 16). The second method involves measuring x-rays emitted from the target surface when irradiated by energetic electrons. The maximum energy x-ray photon is equal to the landing energy of the incident electron. Thus, if the incident electron energy is known and an x-ray spectra is collected, the target potential is determined (17; 18). Each method has been analyzed individually in the literature and each method has unique strengths and limitations. This work considers the fusion of data from both methods to generate an estimate of the electrostatic potential with higher accuracy and lower uncertainty than either method could provide independently. Rather than using only one of the methods, this paper demonstrates that future missions could incorporate both sensors into an electrostatic characterization suite for more robust sensing capabilities. Furthermore, both instruments could be incorporated without adding significant complexity or requirements to the servicing spacecraft. Both x-ray and electron analyzers have extensive flight heritage. It is emphasized that this work is not proposing new hardware, but rather using existing hardware in a novel way to obtain useful information in the context of orbital robotics missions. By using both types of sensors in a collaborative implementation, a target can be electrostatically characterized better than what would be possible with just one type of sensor. The remainder of the paper is structured as follows. Section 2 discusses each method individually, including detailed theory, advantages, and limitations. Section 3 presents experiments to test each method, along with data processing approaches, and uncertainty quantification. Finally, Section 4 discusses fusion of the electron and x-ray data.

2. BACKGROUND AND THEORY

Electron Method

When an energetic electron impacts a surface, it produces additional electrons, known as secondary electrons, which are emitted from the surface at energies of a few eV. The peak of the secondary electron initial energy distribution is equal to one-third the work function of the surface material (19). The number of secondary electrons produced for a single incident electron is known as the secondary electron emission (SEE) yield. It depends on the incident energy and angle
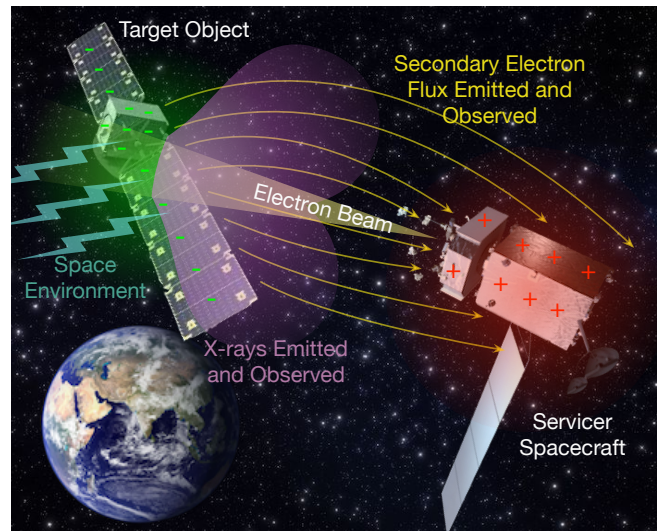
Figure 1. Concept of operations for touchless potential sensing. A servicing craft approaches an object of interest. Secondary electrons and x-rays are generated on the surface of the object by an electron beam, and by the space environment. The servicing craft measures the emitted electrons and x-rays to determine the electrostatic potential of the object.

and is different for every material. For many materials, there is a range of incident energies for which the SEE yield exceeds unity, indicating that a single incident electron causes multiple electrons to be emitted. The SEE yield typically increases as the incident beam becomes more off-normal to the surface (20). This is because for off-normal angles, the incident particles deposit more energy closer to the surface where the secondary electrons have a greater chance of escaping the material.

The electron method for remote sensing leverages the fact that secondaries are generated with very small initial energies. A servicing craft approaches the object of interest and achieves a positive voltage relative to it by emission of an electron beam. Depending on the application, the electron beam may be directed toward the object to transfer charge (for charged actuation, for example) or off into space. Secondary electrons are generated on the surface of the target object either by the active electron beam or by ambient plasma currents in GEO. They are then accelerated by the electric field toward the servicing spacecraft where they are observed with an electron energy analyzer. The energy of the electrons is equal to the potential difference between the two craft. Therefore, if the voltage of the servicing craft is known, the voltage of the object of interest is determined.

The prospects and challenges of the electron method for remote potential sensing are discussed in Reference (15), but are briefly reviewed here. The electron method promises excellent resolution because secondary electrons are generated with initial energies of only a few eV, regardless of the incident particle energy. Electron energy analyzers are ubiquitous on satellites and therefore have extensive flight heritage. Though the focus of this paper is on secondary electrons, photoelectrons are also generated with very small initial energies when a surface is in sunlight. These could similarly be used to remotely sense the voltage of a surface, so

there are both active or passive options for electron sensing. There are some limitations, however. First, a sufficient number of electrons must be generated such that the energy analyzer can detect the signal above the ambient plasma background. Reference (15) demonstrates that, for several different representative flight scenarios, the signal generated from a target spacecraft is sufficiently large to be measured relative to the background plasma, especially because the signal consists of electrons with discrete energies, whereas the background contains a spectrum of energies. Second, the electron trajectories are determined by the electric field in between the two craft. For common spacecraft shapes like boxes and panels, the electric field is directed away from the flat surface except near the edges. Therefore, the electrons generated at a certain point on the target may not fly toward the sensing craft unless the sensing craft is near the line normal to the surface. Given the objects in GEO are commonly tumbling, there may be many times and relative attitudes for which the target voltage is unobservable using the electron method. This effect can be mitigated by defocusing the incident electron beam to illuminate the entire visible side of the target, ensuring that some electrons are always generated at a location that maps back to the sensor.

An example secondary electron spectrum collected by a retarding potential analyzer (RPA) is shown in Figure 2. To obtain this data, an electron beam was directed at an aluminum plate which was held at a fixed potential of -511 V (indicated by the dashed vertical line in both panels). The RPA consists of two metallic grids in front of a collector. The front grid is grounded and a discriminating voltage is applied to the second grid to exclude electrons with energies less than the discriminating grid voltage. The top panel of Figure 2 shows the current-voltage curve. Taking a derivative of this gives the actual electron energy distribution, as shown in the lower panel. A Gaussian curve is fit to the electron energy distribution data and the peak of the curve is taken as the estimate of the plate potential. For the example shown, the estimated voltage is -518 V whereas the actual plate voltage was -511 V. This gives an error of 1.37%. The 95% confidence bounds on the Gaussian fit are taken as the uncertainty associated with the measurement. The noise floor of the electron energy distribution is 0.0605 nA/eV whereas the peak of the Gaussian model is 1.308 nA/eV, giving a signal-to-noise ratio of 21.6. As the total signal received by the RPA decreases, the peak height of the energy distribution tends toward the noise floor and the uncertainty bounds increase toward infinity. Therefore, the measurement is effectively weighted in the filtering algorithm by the height of the peak compared to the noise floor.

Several systematic errors contribute to the accuracy of the electron method. First, the RPA is ultimately a velocity filter, not an energy filter. Though it excludes particles with energies less than the discriminating voltage, it can also exclude particles with higher energies if those particles are not moving along the axis of the instrument (i.e., normal to the grids). Off-axis particles are rejected when the voltage on the grid is lower than their total energy. Thus, any misalignments in the system cause the electron energy distribution to appear to shift to lower energies. The shift in energy is given by the following equation (21):

$$\frac{\Delta E}{E} = \sin^2 \theta, \qquad (1)$$

where θ is the off-axis angle of the particles. Even though the aperture of the RPA is pointed directly at the electron beam spot on the plate, the electric field from the plate and
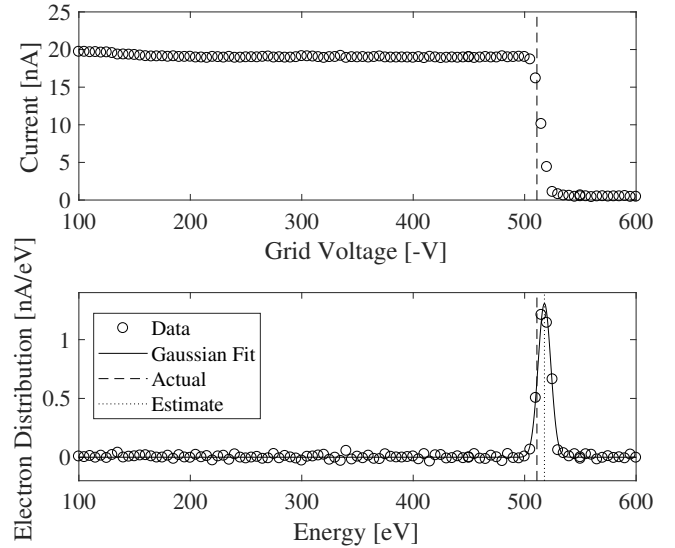
Figure 2. Example electron spectrum generated by a 10 keV, 10 μA electron beam incident on an aluminum plate. The top panel shows the collected current as a function of discriminating grid voltage. The lower panel shows the electron distribution, Gaussian fit, and estimated voltage (dotted vertical line). The dashed vertical line gives the actual plate voltage.

ambient magnetic field can steer the particles such that they enter the RPA at an angle. The ambient magnetic field in the vacuum chamber is on the order of 40 μT. For a 500 eV electron, this gives a gyroradius on the order of 1.9 m whereas the diameter of the chamber is only 0.56 m and the separation distance between the plate and the instrument aperture is only 0.25 m. Another factor is caused by the finite dimensions of the RPA grids which create imperfect equipotential planes because the voltage in the center of a grid square is less than the voltage applied to the actual grid wires (21). This causes a broadening of the electron peak, which for the RPA used in the experiments, results in an increase of the peak width of $\frac{\Delta E}{E} = 2.1\%$. The secondary electrons are generated with a small initial energy distribution which also contributes to the peak location and width. Finally, contaminants and oxide layers on the target surface and cause small, localized potential variations on the order of a volt which affect the measured plate potential (22).

Though in this case the estimate is slightly larger (in magnitude) than the actual plate voltage, this is not always the case. The measurement is affected by the alignment of the RPA relative to the particle flight directions, the design of the RPA, and the surface conditions of the target. Recent experimental campaigns have shown that the electron method is accurate to within a few percent error for a wide range of test conditions and there is not a systematic bias to estimate higher or lower (16).

X-ray Method

As electrons interact with electric fields around atomic nuclei, they undergo accelerations. Each loss of kinetic energy is emitted as a photon in a continuous spectrum, through a process known as bremsstrahlung. The upper limit of the energy that can be radiated in a single interaction is equal to the initial kinetic energy of the electrons, which provides a
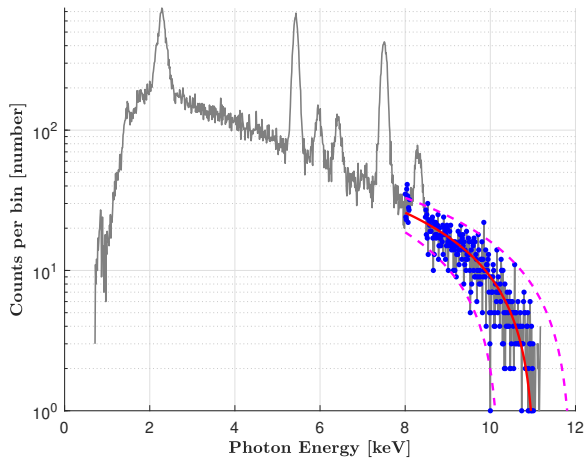
Figure 3. Example x-ray spectrum generated by 11 keV electrons on an inconel target. The peaks are caused by characteristic elemental transitions, while the red line is fit to the blue points to determine the landing energy of the electrons.

Figure 4. Schematic of the experimental setup in the vacuum chamber.

means to determine the landing energy of the electrons (23). The electrons can take an infinite number of trajectories in the vicinity of the nucleus, such that every photon energy up to the landing energy of the electrons is emitted. A continuous x-ray spectrum is formed, as each x-ray observed corresponds to a specific interaction between an atom and an incident electron. If the initial energy of the electrons is known, whether from a servicing spacecraft's electron beam, or the ambient plasma environment, the potential difference between a servicer and a target can then be inferred based on the change in energy of the electrons. The viability of this concept for spacecraft potential determination is theoretically explored in (17), while preliminary experiments are presented in Reference (18). This study determines that determining the landing energy of a beam to less than 1% error is readily achievable using commercially available detectors with prior flight heritage.

As seen in Figure 3, the landing energy can be determined by fitting a line to the upper energy part of the sensed x-ray spectrum. The intercept between the line and the x-axis is then taken to be the landing energy of the electrons, in a method proposed in Reference (24). This method is less sensitive to extraneous x-ray sources or noise than simply taking the highest energy photon collected to be the landing energy, resulting in a more robust estimate of landing energy.

The bremsstrahlung radiation is directionally dependent, which impacts the accuracy of the sensed landing energy. Likewise, there are limits to the physical sensors used to observe the x-ray spectrum. An Amptek X123 Si-PIN diode detector was utilized for these experiments, as this detector is highly compact, requires no external cooling, has prior flight heritage, and has a very good energy resolution of 120 eV. These sensors consist of a beryllium front window, which filters out photons with less than a set energy, preventing detector saturation due ambient illumination. However, detector saturation can still occur for high x-ray count rates, which can be a limiting factor in how quickly a spectrum can be collected. Once the photon enters the Si-PIN diode of the detector, it generates a series of electron-hole pairs.
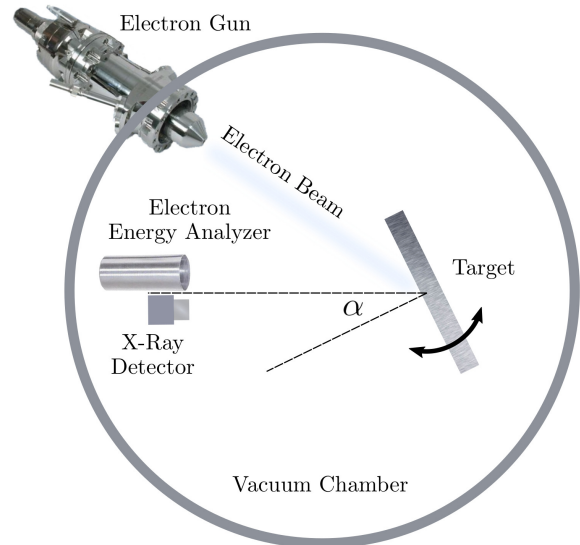
An electric field through the detector then draws the free electrons towards an anode, where they are counted and the number of electrons used to determine the energy of the initial photon, since 3.6 eV is required for each electron-hole pair generated. The landing energy uncertainty is determined from a statistical assessment of the line of best fit, by adding bounding lines to cover 95% of the sampled data points. The x-intercepts of these bounding lines are then used to establish bilateral uncertainties.

Over longer collection periods, the detector can experience drift, likely due to thermal impacts on the sensor. These issues impact the calibration of the detector, such that characteristic peaks appear to move. Because these are known constant energies, they can be used to re-calibrate the measured spectrum after collection to ensure that the characteristic peak locations are consistent.

3. EXPERIMENTAL SETUP

Previous studies (18; 25; 16) have experimentally investigated both methods for potential estimation, though each method was considered individually. In this study, new experiments are conducted which facilitate fusion of electron and x-ray data for experimental investigation of the combined sensing technique. Specific experimental conditions which span the regions of observability for each method are selected. Data was collected in a space environment simulation chamber at the University of Colorado Boulder. Figure 4 shows a schematic of the experimental setup in the vacuum chamber, while Figure 5 shows a picture of the experiment as constructed. A Kimball Physics EMG-4212 electron gun was used to irradiate an aluminum target plate, generating secondary electrons and x-rays. The target plate was mounted on a rotating stage controlled by a stepper motor. The plate was held at a fixed potential by a high voltage power supply. An Amptek X-123 x-ray spectrometer with a Si-PIN detector was used to observe the x-rays. This device has prior flight heritage on the MinXSS smallsat solar observatory mission, and has a mass under 180g, including control electronics, and
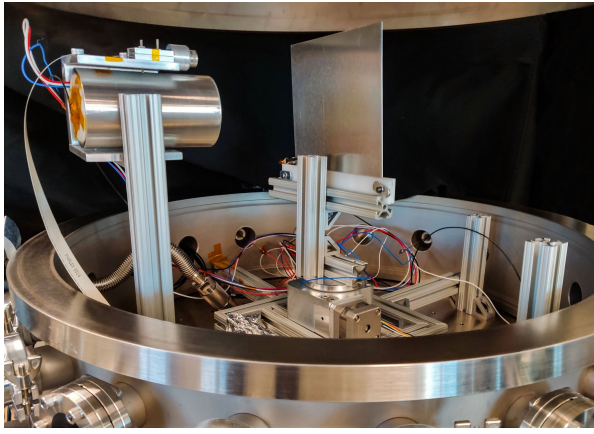
Figure 5. Picture of experimental setup inside vacuum chamber. The target plate is to the right, while the x-ray detector is mounted on top of the RPA to the left. The target plate is mounted to a rotary stage.

the actual sensor fits into a volume of 3 cm by 2 cm by 1 cm. The sensor and control electronics consume less than 2 watts total. (26) A custom-built retarding potential analyzer (RPA) was used to measure the electrons. The RPA is cylindrical, approximately 15 cm in length and 8 cm in diameter, though flight versions have been designed to be smaller, with masses of less than 1 kg and power consumptions of less than 5 watts (27). A Keithley 2401 picoammeter recorded the secondary electron current.

In the first experiment, both the target plate and instruments were held at fixed positions. A known voltage was applied to the plate and data was collected for 1 hour and the application of a steady-state Kalman filter to fuse the two data streams investigated. In the second experiment, the instruments were held at a fixed location and the plate was rotated through 360°, which simulates the tumbling dynamics of many on-orbit satellites of interest. While the plate was only rotated about one axis here, similar results would be expected if the plate were rotated about the second axis instead. The results of these experiments are discussed in the following sections. Here, the core methods of potential estimation are being extended to combine results from both methods to create a more accurate estimate of the target potential. Additionally, this fusion is experimentally validated and tested with time-varying target potentials.

4. FUSION OF POTENTIAL ESTIMATES

Each of the proposed methods has unique strengths and limitations, which makes fusing the data from each sensor appealing. Bremsstrahlung emission has a high level of directional dependence, with the intensity and shape of the spectrum varying as a function of the angle from the incident electron beam. Prior work demonstrates that the bremsstrahlung method accuracy varies as a function of the angle between the detector and the incident beam, for a given beam energy. The secondary electrons likewise have an angular distribution that affects the collected yield at a given position, but this angle is relative to the local surface normal. In an operational scenario, the servicer moves relative to the target, and the target is likely to be rotating relative to the servicer. However, the instruments and the electron beam would be mounted

at fixed points on the servicer. This results in a constant angle between the sensors and the electron beam, so the x-ray sensor will always be observing the same portion of the bremsstrahlung spectrum. The orientation relative to the target's surface will be varying with time however, so the secondary electron yield observed changes significantly.

Prior experimental work has demonstrated that the x-ray method tends to have higher uncertainties in the measured quantities than the secondary electron method, largely due to the increased noise sources in the x-ray sensor compared to the RPA. However, an x-ray spectrum could be collected in as little as a second, whereas electron spectra likely take longer because of the need to sweep through voltages. For the power supplies used in these experiments, an electron spectrum requires on the order of a minute. Each method therefore has unique strengths which allow them to be used in a complimentary fashion.

Two experiments were set up to demonstrate the potential for fusing the two types of measurements. First, a constant potential of -900V was maintained on a flat 6061 aluminum target, and both electron and x-ray spectra collected every minute for an hour. The collection time for both instruments can be reduced. Here, 20 second integrations were used for the x-ray detector, and the RPA control electronics required approximately 45 seconds to sweep through the full range of potentials investigated. The size of the voltage steps used for the RPA could be increased, resulting in a faster, but more uncertain estimate of the electron peak location. Reducing the integration time for the x-ray detector results in fewer photons being collected and a noisier estimate of the landing energy. One minute update periods were chosen here to allow the controlling equipment adequate time to process and save the data from each sensor before the next collection, but this could be decreased in the future.

The estimated potentials are then fused using a steady-state Kalman filter, which had an initial estimate of 0 V. Figure 6 illustrates the data collected by both instruments, and the uncertainty associated with each measurement. While uncertainties are fairly similar between the two types of measurement, the SEE data is noticeably more consistent than the bremsstrahlung data (as can also be seen in Figure 7). However, this data exhibits a constant offset of +30V relative to the true plate potential for this case. This offset is not present in every data set. From Equation 1, it is likely that this steady state offset is caused by an approximately 10° difference between the trajectory of the secondary electrons and the axis of the RPA.

For a given space environment condition, spacecraft reach an equilibrium potential very quickly (seconds or less). However, the charge state evolves on the order of hours, as space weather conditions change. On-orbit charging involves a range of current sources, dominated by interactions with plasma electrons, ions, photoelectrons and the backscattered and secondary electrons associated with those currents. All of these currents are highly dependent on material properties and the spacecraft surface potential, which makes developing an accurate dynamic model of the charging very challenging. If an active electron beam is used for forced charging, it is a good assumption that the beam dominates the other ambient currents and determines the ultimate charge on the target.

However, after reaching an equilibrium potential, spacecraft tend to vary in potential quite slowly, such that a steady state approximation could be applied in filter development in the

absence of a higher fidelity model. The goal of this work is to investigate fusion of data from the two sensing methods to improve the potential estimate in a steady-state situation. Future work will apply these techniques to time-varying surface potentials, such as those that have been observed at GEO.

The system state matrix, A, is equal to identity for the steady-state case. The states and the system state matrix are both scalars since only the target potential is to be estimated. The measurement vector, z, consists of the x-ray measurement and electron measurement for a given timestep stacked into a 2×1 vector. The measurements are directly equal to the state of interest, so the measurement-to-state conversion matrix H is a 2×1 vector of ones. The process noise matrix Q (in this case a scalar quantity) is manually tuned, and good filter performance occurs when Q is set to identity.

For each timestep, the filter is updated according to the algorithm below. First, the predicted estimate is computed as the prior state estimate:

$$Xp_i = AX_{i-1} \tag{2}$$

The scalar error covariance is then predicted, using the state dynamics, the prior covariance, and the process noise.

$$Pp_i = AP_{i-1}A^T + Q \tag{3}$$

Then the Kalman gain for this step (which has dimensions 1×2) is computed as

$$K_i = Pp_iH^T(HPp_iH^T + R)^{-1} \tag{4}$$

Which leads to the computation of the updated state estimate

$$X_i = Xp_i + K_i(z_i - HXp_i) \tag{5}$$

And finally, the scalar error covariance is updated

$$P_i = Pp_i - K_iHPp_i. \tag{6}$$

Ultimately, the filter converged to -895 volts with a covariance of ±18V with fewer than 20 measurements, significantly outperforming either of the individual sensing methods. The residuals in Figure 7 illustrate that the error for the fused method is lower than the errors seen by either of the individual methods, although it does have a non-zero mean due to the consistent offset from the SEE data. The time to convergence (for this case defined by the estimate reaching within 5% of the true plate potential) could be reduced by adjusting the filter gains, initializing with a better guess, or, filter parameters remaining constant, by increasing the sample rate of the measurements. Decreasing the time between measurements or the uncertainty associated with them would allow for the filter to converge on the true value in less time.

While this demonstrates some of the advantages of filtering and fusing the two data sources in a static scenario, the second experiment highlights some of the significant advantages combining both methods can present for rotating targets. This experiment consists of the same aluminum plate mounted to a rotational stage, while the sensors are in a fixed position inside the chamber. The potential of the plate is held at -511 V by a high voltage power supply, and the plate potential is held constant while the plate rotates. This is analogous to a flight scenario, where the sensors are in a fixed position relative to the electron beam, but the angle relative to the
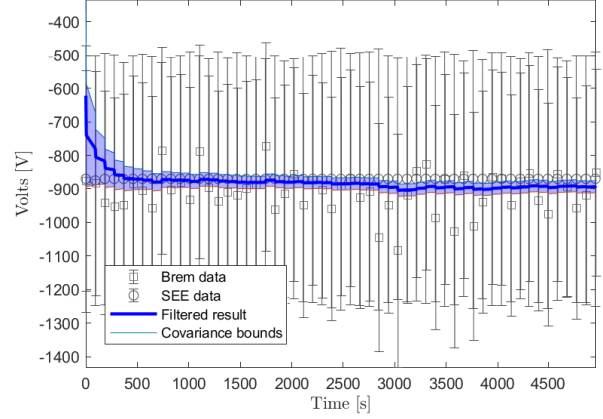
Figure 6. Measurements and uncertainties for electron and x-ray observations of a fixed plate at a steady-state voltage of -900 V. The solid blue line shows the result for the fused data set and the shaded blue regions depict the covariance bounds.
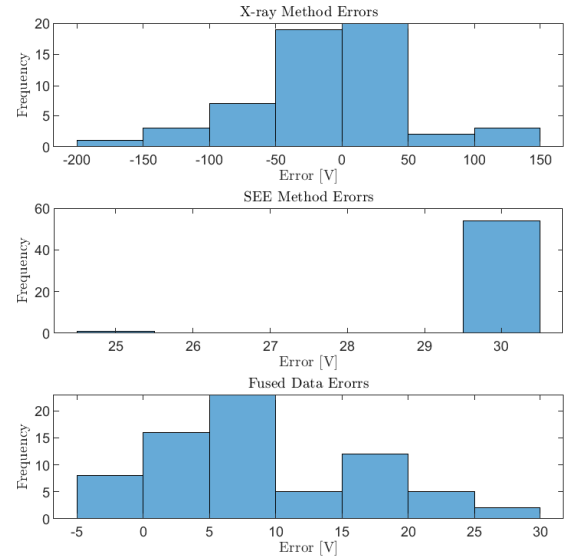
Figure 7. Histogram of errors for the x-ray estimated potential, electron-estimated potential and the fused result.

target is time-varying. In this experiment, the target was held stationary while electron and x-ray spectra were collected. After collecting a spectrum at a given point, the plate was rotated by $5°$, and a new spectrum of each type collected. The plate angle is defined as the angle between the plate normal and the instrument positions. Therefore, angles of $0°$, $180°$, and $360°$ indicate that the plate is facing the instruments. The electron gun parameters were held constant throughout the experiment at 10 keV emission energy, and a beam current of $10\,\mu A$.

For some target plate angles, additional characteristic peaks were observed. These were found to correspond to iron and chromium, indicating that the electron beam was impacting
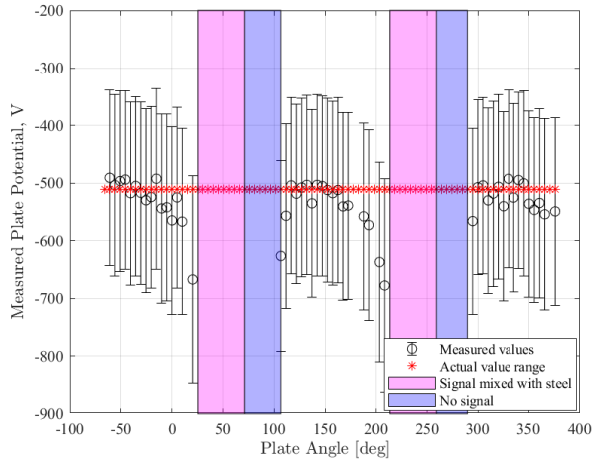
Figure 8. Estimated plate potential as a function of angle using x-ray method.

Figure 9. Uncertainty in plate potential determination as a function of target plate angle

Figure 10. Steady state Kalman filter applied to x-ray data, SEE data and fused data.

not only the target, but the chamber walls as well. While the plate was held at a fixed non zero potential, the chamber walls were grounded, so the bremsstrahlung spectrum would be a combination of contributions of electrons with two different landing energies. Therefore, runs with characteristic peaks of iron and other elements not found in the 6061 aluminum target plate were discarded. Future work aims to resolve multiple electron landing energies in a single bremsstrahlung spectrum, but the method applied here is valid for only one. In a space scenario, the portion of the electron beam which does not hit the target will instead continue off into space, resulting in reduced, but uncontaminated, x-ray spectrum from the target. The regions in this test where both aluminum and steel signatures were observed are highlighted in Figure 8.

For these cases the electron beam was impacting only the aluminum target for 56% of the plate's rotation. Another 21% of the positions yielded a mix of signals from the chamber walls and the target plate and had to be discarded, while the remaining 23% were very low signal yields that made material identification and landing energy determination unreliable. The regions of each type of signal are shown in Figure 8.

The steady-state Kalman filter described earlier was applied to both the x-ray and the SEE data from the rotating target test, and then to the combination of both data sets. The fused results outperformed the results for either data source on its own, as seen in Figures 10 and 11, but the most significant gains are seen in maintaining an accurate solution through angles. It is possible to obtain a signal from at least one of the methods through almost all angles, even with the x-ray measurements being limited due to the electron beam impinging on the chamber walls. Without these contaminating cases, a usable x-ray spectrum would be observed in over 75% of cases, with fairly consistent uncertainties and errors (as seen in Figure 9).

While the SEE data provides a highly accurate solution with low uncertainties when the geometry is optimally oriented, the confidence in the computed solution quickly decreases for off-normal geometries because no electron signal is actually measured. The uncertainty from the x-ray method is large
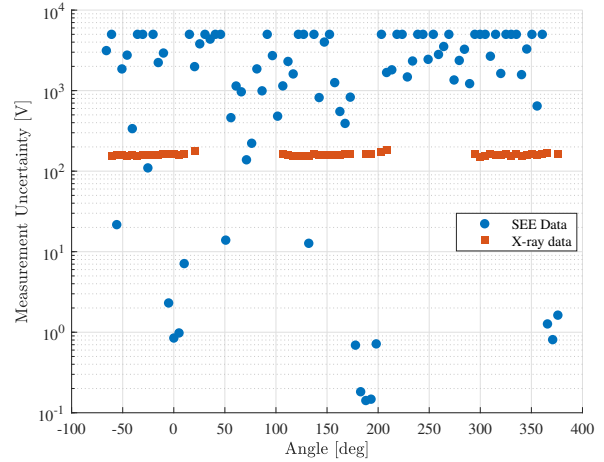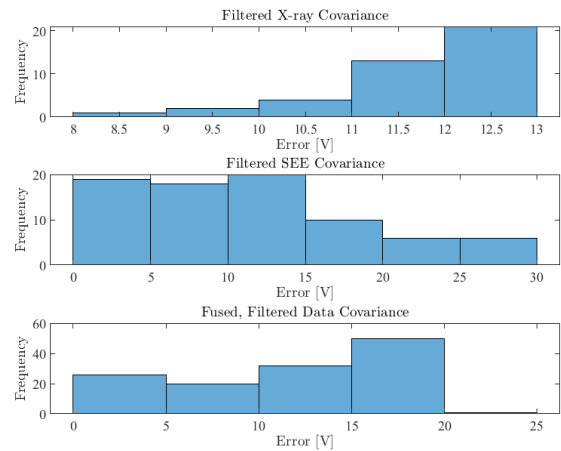
in the best cases, but varies far less as the target rotates. The relationship between angle and uncertainty for the -511V plate case is illustrated in Figure 9.

Figure 12 shows the mean collected electron current as the target plate rotated through a full revolution for several plate voltages, with a constant set of electron beam parameters (10 keV, 10 μA). Note that a measureable peak in the electron data is only obtainable if the total signal is greater than 0.8 nA. During each test, the total signal exceeded this threshold 17% of the time. Therefore, the SEE method only produces quality measurements for a narrow range of angles near the plate normal. As with the prior cases, the plate is rotated through a full 360°, so angles of 0°, 180°, and 360° indicate the plate is facing the detector.

7
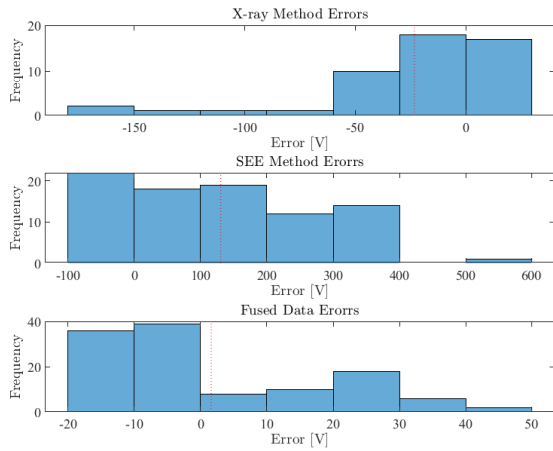
Figure 11. Histogram of errors for each measurement method, and the fused, filtered result. Two additional SEE runs had errors of -1297V and -2805V, but are not shown on the histogram.
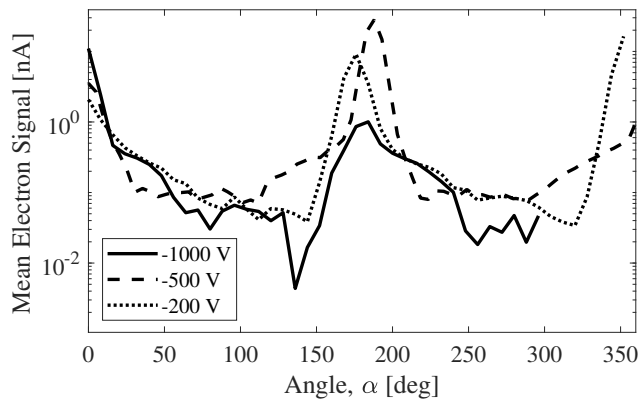
Figure 12. Mean SEE signal as a function of angle between the plate normal and the instrument location for various voltages.

5. CONCLUSION

Two methods for remote sensing of spacecraft electrostatic potential have been evaluated in a series of vacuum chamber experiments. The electron method produces highly accurate measurements of the target potential with small uncertainties when the detector is near the line normal to the target surface. As the plate rotates so the electron detector is off the normal axis, the electron current quickly drops to zero and no measurement is obtained. The x-ray method has the advantage of being agnostic to the geometry of the target surface, but generally produces measurements with larger uncertainties. Further, the x-ray method does not place any requirements on the relative potentials of the two objects, whereas the electron method only works if the electrons are accelerated toward the servicing satellite. Fusing the datasets using a steady state Kalman filter mitigates the limitations of each instrument, thereby producing an estimate of the plate potential with smaller errors and uncertainties. Despite these advances, there remain numerous avenues for future work.

Only plate geometries (representative of spacecraft solar panels, for example) have been considered so far, but more complex targets, such as a box with panels will have more complicated electric fields which will further affect the measurements. Additionally, spacecraft often experience differential charging, in which different parts of the spacecraft charge to different potentials. This effect significantly complicates the measurement process for both methods. In a flight implementation, ambient plasma electrons will contaminate the electron spectrum, and hot ambient electrons will also generate bremsstrahlung radiation on the target surface. While these effects are expected to be small relative to the anticipated current and x-ray fluxes from the target, these impacts should be analyzed more carefully. Intermittently pulsing the electron beam would allow the background spectrum in both x-rays and electrons to be determined, which may improve the ability to reject such noise sources from measurements. Finally, the separation distance and scale of the target is limited due to the finite volume of the vacuum chamber. Simulations must be used to consider how the sensing methods vary with separation distance. Ultimately, continued research along these lines will advance the remote characterization concept that will be highly useful for future on-orbit proximity operations missions.

6. ACKNOWLEDGEMENT

REFERENCES

[1] P. C. Anderson, "Characteristics of spacecraft charging in low earth orbit," *Journal of Geophysical Research: Space Physics*, vol. 117, no. A7, 2012.

[2] E. Mullen, M. Gussenhoven, D. Hardy, T. Aggson, B. Ledley, and E. Whipple, "Scatha survey of high-level spacecraft charging in sunlight," *Journal of Geophysical Research: Space Physics*, vol. 91, no. A2, pp. 1474–1490, 1986.

[3] S. T. Lai, *Fundamentals of spacecraft charging: spacecraft interactions with space plasmas*. Princeton University Press, 2011.

[4] B. B. Reed, R. C. Smith, B. J. Naasz, J. F. Pellegrino, and C. E. Bacon, "The restore-l servicing mission," in *AIAA SPACE 2016*, 2016, p. 5478.

[5] B. Sullivan, D. Barnhart, L. Hill, P. Oppenheimer, B. L. Benedict, G. Van Ommering, L. Chappell, J. Ratti, and P. Will, "Darpa phoenix payload orbital delivery system (pods):"fedex to geo"," in *AIAA SPACE 2013 conference and exposition*, 2013, p. 5484.

[6] D. Barnhart, B. Sullivan, R. Hunter, J. Bruhn, E. Fowler, L. M. Hoag, S. Chappie, G. Henshaw, B. E. Kelm, T. Kennedy *et al.*, "Phoenix program status-2013," in *AIAA SPACE 2013 conference and exposition*, 2013, p. 5341.

[7] M. Goodman, A. Paez, E. Willis, and A. DeStefano, "An analytic model for estimating the first contact resistance needed to avoid damaging esd during spacecraft docking in geo," in *Applied Space Environments Conference*, 2019.

[8] C. Jewison, D. Sternberg, B. McCarthy, D. W. Miller, and A. Saenz-Otero, "Definition and testing of an architectural tradespace for on-orbit assemblers and ser-

vicers," 2014.

[9] M. Bengtson, K. Wilson, J. Hughes, and H. Schaub, "Survey of the electrostatic tractor research for reorbiting passive geo space objects," *Astrodynamics*, vol. 2, no. 4, pp. 291–305, 2018.

[10] V. Aslanov and V. Yudintsev, "Motion control of space tug during debris removal by a coulomb force," *Journal of Guidance, Control, and Dynamics*, vol. 41, no. 7, pp. 1476–1484, 2018.

[11] V. Aslanov and H. Schaub, "Detumbling attitude control analysis considering an electrostatic pusher configuration," *Journal of Guidance, Control, and Dynamics*, vol. 42, no. 4, pp. 900–909, 2019.

[12] T. Bennett and H. Schaub, "Touchless electrostatic three-dimensional detumbling of large axi-symmetric debris," *The Journal of the Astronautical Sciences*, vol. 62, no. 3, pp. 233–253, 2015.

[13] Y. S. Karavaev, R. M. Kopyatkevich, M. N. Mishina, G. S. Mishin, P. G. Papushev, and P. N. Shaburov, "The dynamic properties of rotation and optical characteristics of space debris at geostationary orbit," *Advances in the Astronautical Sciences*, vol. 119, 2004.

[14] D. Stevenson and H. Schaub, "Multi-sphere method for modeling electrostatic forces and torques," *Advances in Space Research*, vol. 51, no. 1, pp. 10–20, Jan. 2013.

[15] M. Bengtson, J. Hughes, and H. Schaub, "Prospects and challenges for touchless sensing of spacecraft electrostatic potential using electrons," *IEEE Transactions on Plasma Science*, 2019.

[16] M. Bengtson, K. Wilson, and H. Schaub, "Simulations and experimental results of electron method for remote spacecraft charge sensing," in *Applied Space Environments Conference*, 2019.

[17] K. Wilson and H. Schaub, "X-ray spectroscopy for electrostatic potential and material determination of space objects," *IEEE Transactions on Plasma Science*, 2019.

[18] ——, "Electron-induced x-rays for remote potential sensing," in *Applied Space Environments Conference*, 2019.

[19] M. Chung and T. Everhart, "Simple calculation of energy distribution of low-energy secondary electrons emitted from metals under electron bombardment," *Journal of Applied Physics*, vol. 45, no. 2, pp. 707–709, 1974.

[20] H. Bruining, "Physics and applications of secondary electron emission," 1954.

[21] C. Enloe, "High-resolution retarding potential analyzer," *Review of scientific instruments*, vol. 65, no. 2, pp. 507–508, 1994.

[22] S. Robertson, Z. Sternovsky, and B. Walch, "Reduction of asymmetry transport in the annular penning trap," *Physics of Plasmas*, vol. 11, no. 5, pp. 1753–1756, 2004.

[23] W. Duane and F. Hunt, "On x-ray wave-lengths," *Phys. Rev.*, vol. 6, pp. 166–172, Aug 1915. [Online]. Available: https://link.aps.org/doi/10.1103/PhysRev.6.166

[24] P. C. M. Lamoureux, "General deconvolution of thin-target and thick-target bremsstrahlung spectra to determine electron energy distributions," *Radiation Physics and Chemistry*, vol. 75, no. 10, October 2006.

[25] M. Bengtson and H. Schaub, "Remote sensing of spacecraft potential at geosynchronous orbit using secondary and photo electrons," in *AIAA Scitech 2019 Forum*, 2019, p. 0311.

[26]

[27] L. Fanelli, S. Noel, G. D. Earle, C. Fish, R. L. Davidson, R. V. Robertson, P. Marquis, V. Garg, N. Somasun-daram, L. Kordella, and P. Kennedy, "A versatile retarding potential analyzer for nano-satellite platforms," *Review of Scientific Instruments*, vol. 86, no. 12, p. 124501, 2015.

BIOGRAPHY

Kieran Wilson is a graduate research assistant at the University of Colorado Boulder in the Aerospace Engineering Sciences Department. He received B.S. degrees in Aerospace Engineering and Mechanical engineering from the University of Florida in Gainesville, FL. Kieran's research interests include charged astrodynamics, and attitude determination and control systems.

Miles Bengtson is a graduate research assistant and NDSEG Fellow at the University of Colorado Boulder in the Aerospace Engineering Sciences Department. He graduated with distinction with M.S. and B.S. degrees in Engineering Physics from Embry-Riddle Aeronautical University in Daytona Beach, FL. Miles is a former Space Scholar at the Air Force Research Laboratory, a member of the AIAA Atmospheric and Space Environments Technical Committee, and an alumnus of the International Space University. His research interests include spacecraft-plasma interactions, charged astrodynamics, and experimentation.

Hanspeter Schaub Dr. Schaub is the Glenn L. Murphy Chair of Engineering at the University of Colorado and is the current graduate chair of the Aerospace Engineering Sciences department. He has over 20 years of research experience, of which 4 years are at Sandia National Laboratories. His research interests are in nonlinear dynamics and control, astrodynamics, relative motion dynamics, as well as relative motion sensing. In the last decade he has developed the emerging field of charged astrodynamics. Dr. Schaub has been the ADCS lead in the CICERO mission and the ADCS algorithm lead on a Mars Mission. He is an AAS and AIAA Fellow, and has won the AIAA/ASEE Atwood Educator award, as well as the AIAA Mechanics and Control of Flight award. He currently serves as the Editor-In-Chief for the AIAA Journal of Spacecraft and Rockets.